**IAES International Journal of Artificial Intelligence (IJ-AI)**
Vol. 14, No. 6, December 2025, pp. 4623~4635
ISSN: 2252-8938, DOI: 10.11591/ijai.v14.i6.pp4623-4635 

# Low-speed scalar control of induction motor by fuzzy logic

**Alfonso Alejandro Sevilla-Hidalgo[1], Rossy Uscamaita-Quispetupa[1], Julio Cesar Herrera-Levano[2], Limberg Walter Utrilla Mego[2], Roger Jesus Coaquira-Castillo[1]**
[1]LIECAR Laboratory, Faculty of Electrical, Electronic, Computer and Mechanical Engineering, Universidad Nacional de San Antonio Abad del Cusco, Cusco, Peru
[2]TESLA Laboratory, Faculty of Electrical, Electronic, Computer and Mechanical Engineering, Universidad Nacional de San Antonio Abad del Cusco, Cusco, Peru

**Article Info**

***Article history:***

Received Mar 15, 2025
Revised Oct 01, 2025
Accepted Oct 16, 2025

***Keywords:***

Fuzzy controller
Low speeds
PI controller
Three phase induction motor
V/f scalar control

**ABSTRACT**

Efforts have continually been directed toward optimizing processes in various fields, and the application in induction motors is no exception. Scalar control V/f offers a straightforward method to regulate the speed of a three-phase induction motor (TIM). However, it faces challenges at low speeds or proportionally at low frequencies, often failing to operate below 20% of its rated speed. This control typically pairs with a PI controller (PIC) for closed-loop speed regulation, but its limited control range hinders performance at low speeds. Although intelligent methods have been developed to improve scalar V/f control, attention is often focused on high speeds, while control at low speeds is overlooked. This paper presents the simulation of a fuzzy controller (FC) with a Mamdani-type structure designed to achieve effective low-speed control of a TIM using the V/f scalar control technique. The results not only show improvements in overshoot and settling time but also reveal that the FC can control speeds as low as 6.06% of the rated speed, and it ensures a starting current below the designed motor current under load. Comparative analysis indicates that the FC outperforms the PIC in low-speed control, and it provides an optimal inrush current across different low speeds.

*This is an open access article under the CC BY-SA license.*

***Corresponding Author:***

Roger Jesus Coaquira-Castillo
LIECAR Laboratory, Faculty of Electrical, Electronic, Computer and Mechanical Engineering
Universidad Nacional de San Antonio Abad del Cusco
La Cultura Avenue 733 Cusco, Cusco, Peru
Email: roger.coaquira@unsaac.edu.pe

## 1. INTRODUCTION

The use of direct current (DC) motors has declined in various applications, including electric and hybrid vehicles and railway systems [1], [2]. As a result, the three-phase induction motor (TIM) has been preferred over DC motors due to its ease of maintenance, high reliability, cost-effectiveness, simple design, robust durability, and excellent power-to-weight ratio [3]. Consequently, there has been growing interest in advanced control techniques, primarily V/f scalar control and vector control.

It is noted that V/f scalar control is chosen for its simplicity, practicality, and cost-effectiveness [4], although it struggles at low speeds—typically below 20% of the motor's nominal speed—because the flux increases significantly, leading to torque and current surges [5], [6]. Additionally, it is acknowledged that starting currents in TIM can reach up to ten times the rated current [4], [7], [8], increasing risks to electrical components, potentially overloading power systems, and resulting in economic drawbacks [9]. Hence, it is emphasized that methods aimed at achieving an optimal peak starting current and a suitable speed response, especially at low frequencies, are essential for improved motor performance.

PI controllers (PICs) have been frequently employed in V/f scalar control for speed regulation in TIMs [10], [11], and are reported to be suitable in contexts where a detailed mathematical model is difficult to establish due to resource constraints and complex operations [8], [12]. Their capacity to minimize or eliminate steady-state errors, combined with a simple structure, has been emphasized [13], although their performance is limited in speed response and under load variations [14]. These drawbacks have led to efforts to improve PIC through enhanced techniques [15], [16], yet difficulties remain at low speeds, especially concerning speed response and inrush current management. Consequently, fuzzy logic control has been examined in V/f scalar control for TIMs [17], [18], where it has been recognized for its accuracy and robustness [19]. However, although improvements in transient behavior (overshoot, settling time, and rise time) have been identified, the advantages of fuzzy controllers (FC) at low speeds have received limited attention, as presented in Table 1.

Table 1. Approaches of fuzzy and V/f scalar control in TIMs

| Type of analysis | Advantages | Disadvantages |
|---|---|---|
| Integration of fuzzy logic with variable frequency drive [20]. | Improved energy efficiency, real-time speed adjustment, and reliability and economically beneficial. | High initial costs, dependency on specialized hardware that can lead to accessibility problems. |
| Development of an optimal fuzzy-PIC [21]. | Reduced computational load, improved speed response, reduced rule set, and faster stabilization. | Limited to a specific rpm range (1300-1725 rpm). |
| Fuzzy logic controllers for speed control under fluctuating loads [22]. | Faster adjustment to speed changes, robustness against load disturbances, and simplifies control schemes. | Focus on high speeds (specifically 1000 rpm), potentially limited lower speed performance. |

It is noted that modifying the V/f scalar control can compensate for torque at low frequencies, based on a "Torque boost" approach [23]. Increasing electrical starting torque is essential to overcome mechanical torque, although it induces higher inrush currents, which are a key consideration for motor startup [24]. The equations in [25] show that the starting torque depends on the inrush current.

The possibility of a fuzzy logic-based torque compensation at low frequencies, termed "Current compensation", is considered to achieve a "Torque boost" for TIMs under V/f scalar control. This raises the question of whether such fuzzy logic controller (FLC) can deliver an effective speed response and optimize inrush current below 20% of the rated speed, while retaining the improvements offered by the FC in transient response. Hence, this work aims to enhance the PIC for V/f speed regulation by coupling a PIC with an FLC method. The objective is to optimize low-speed control response, manage inrush current, and enlarge the operational control range [5], [26]. Explicit criteria for speed and current in transient scenarios are established to enable a parameter comparison between the FC and the PIC, conveying mathematical objectivity.

## 2. METHOD

This research involves the development, simulation, and evaluation of a fuzzy-logic–enhanced V/f scalar control scheme for a TIM, leveraging MATLAB/Simulink and Lucas–Nuelle's toolbox. The objective is to provide an AI-based solution to the challenges of scalar V/f control at low speeds. First, the V/f scalar control system was designed; next, negative feedback was implemented using a PIC tuned via particle swarm optimization (PSO). The PIC-based feedback loop was then analyzed to develop a FC-based feedback loop within the scalar V/f framework. Finally, both the PIC and FC schemes were simulated, evaluated, and compared in terms of speed and current responses over a predefined speed range, with particular emphasis on low-speed performance. Figure 1 shows the overall block diagram of the low-speed scalar V/f control system with the FC, detailing the key components and their interactions to provide a complete overview of the system's functionality.

### 2.1. V/f scalar control design

#### 2.1.1. V/f relation

Before establishing the V/f relationship, a scaling factor of 1/30 is introduced so that the synchronous speed, ns, can be handled conveniently in revolutions per minute (rpm). This conversion appears in (1), which is derived from the fundamental synchronous-speed expression shown in (2). In both equations, f denotes the supply frequency (Hz) and P represents the number of motor poles.

$$f = n_s \frac{1}{30} \quad (1)$$

$$n_s = \frac{120f}{P} \tag{2}$$

Under the assumed linear V/f profile, the stator frequency is limited to the 3 Hz–29 Hz interval, which corresponds to a controllable speed range of 100 rpm–800 rpm. An additional tolerance band is specified, narrowing the effective closed-loop range to 90 rpm–870 rpm to ensure reliable operation near the extreme points. Within this band, the modulation signal sent to the insulated gate bipolar transistor (IGBT) control block varies from 5% to 58% of the preset 220 V DC link voltage, since the voltage is normalized to frequency. Consequently, the resulting V/f characteristic is defined by (3), where VV/f is the output voltage determined by the V/f ratio; f is the reference frequency (Hz); A is the reference value corresponding to 100% of the DC link voltage; and fmax is the maximum (normalized) frequency for the V/f ratio.

$$V_{V/f} = \begin{cases} 0, & f < 0 \\ \frac{fA}{f_{max}}, & 0 \le f \le 50 \\ 100, & f > 50 \end{cases} \tag{3}$$

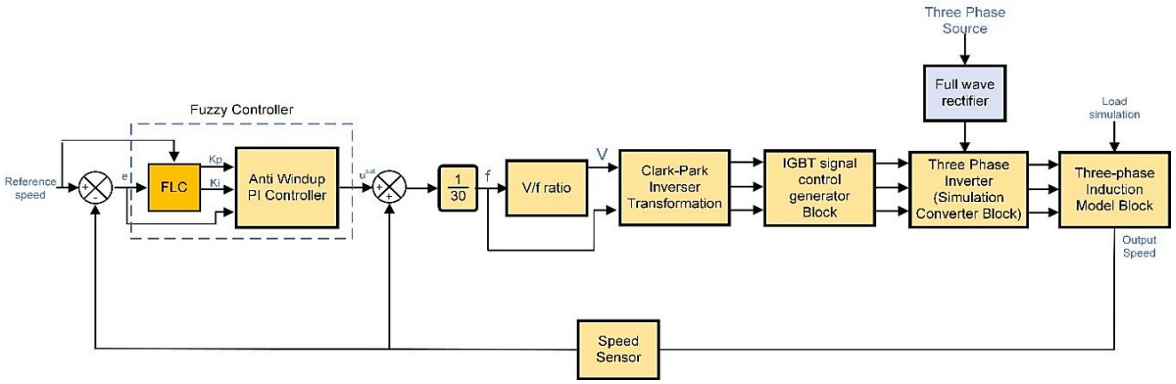


Figure 1. Fuzzy control block diagram

### 2.1.2. Clark-Park transformation

The Clarke–Park transformation is used to obtain three balanced sinusoidal references required by the inverter's modulation stage. To generate the pulse-width modulation (PWM) signals for the inverter implemented with the LN blocks, the IGBT control block must receive three-phase sinusoidal signals that encode both the desired fraction of the preset DC link voltage and the switching frequency demanded by the IGBTs. These requirements are met by first applying the inverse Park transformation to the voltage reference obtained from the V/f ratio. The matrix form of the inverse Park transformation is given in (4).

$$\begin{bmatrix} Ds \\ Qs \end{bmatrix} = \begin{bmatrix} \cos(\theta) & -\sin(\theta) \\ \sin(\theta) & \cos(\theta) \end{bmatrix} \begin{bmatrix} V_\alpha \\ V_\beta \end{bmatrix} \tag{4}$$

Here, $V_\alpha$ is set to zero, and $V_\beta$, which stems from the V/f profile, is generated by an LN integrator block that resets every $2\pi$ with a period of 1/f. Once the Ds and Qs components are obtained, a modified inverse Clarke transformation, expressed in (5), is applied to translate these orthogonal voltages into the three-phase references required by the IGBT switches. In (5), Uc, Vc, and Wc constitute the final control signals delivered to the IGBT control block. Each signal simultaneously encodes, in its amplitude, the percentage of the inverter's DC link voltage and, in its frequency, the carrier needed for accurate PWM generation.

$$\begin{bmatrix} U_c \\ V_c \\ W_c \end{bmatrix} = \begin{bmatrix} 1 & 0 & 1 \\ -\frac{1}{2} & \frac{\sqrt{3}}{2} & 1 \\ -\frac{1}{2} & -\frac{\sqrt{3}}{2} & 1 \end{bmatrix} \begin{bmatrix} D_s \\ Q_s \\ 0 \end{bmatrix} \tag{5}$$

### 2.1.3. Three-phase inverter

The three-phase inverter, or simulation converter block, synthesizes the motor phase voltages by switching its insulated-gate bipolar transistors in response to the reference signals. These reference signals are

the standard IGBT control waveforms generated by the IGBT control block with PWM at 8 kHz. During each carrier period, the simulation converter block combines the IGBT control signals, the maximum PWM counter value, and the preset DC-link voltage to compute the instantaneous output voltages delivered to the motor [27]. Here, Vdc is supplied by a full-wave rectifier connected to the three-phase mains.

### 2.1.4. Three-phase induction motor model

The dynamic behavior of the drive is represented through a detailed TIM model. Figure 2 shows the single-phase equivalent circuit that underpins this model. Because the three stator phases are identical and the supply is perfectly balanced, the model derived from one phase can be extrapolated to the full machine. Accordingly, the three-phase induction model block, or induction model block, from the Lucas–Nülle toolbox implements the motor dynamics by numerically solving the fundamental equations listed in (6) to (8).

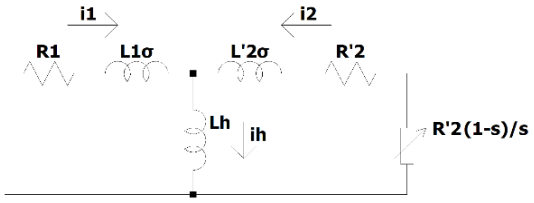


Figure 2. Induction motor monophase equivalent circuit

In (6) expresses the mechanical torque $M_{mech}$ as the ratio between electromagnetic power and rotor speed, whereas in (7) links the electromagnetic torque M and the load torque $M_L$ to the rotor's angular acceleration through its moment of inertia J. In (8) provides a state-space description that simultaneously governs the stator currents ($i_{Sa}$, $i_{Sb}$, and rotor flux linkages ($\Psi_{Ra}$, $\Psi_{Rb}$) in the stationary $\alpha-\beta$ frame, using machine parameters such as Ls, Lr, Lm, Rs, Rr, and the time constants Tσ and $T_R$. Together, these equations capture the electromechanical coupling that defines induction-motor operation.

$$M_{mech} = \frac{P_{mech}}{\omega_m} = \frac{3}{2} z_p \frac{L_m}{L_R} (\Psi_{Ra} i_{Sb} - \Psi_{Rb} i_{Sa}) \tag{6}$$

$$\frac{J d\omega_m}{dt} = M - M_L \tag{7}$$

$$\frac{d}{dt}\begin{bmatrix} i_{Sa}(t) \\ i_{Sb}(t) \\ \Psi_{Ra}(t) \\ \Psi_{Rb}(t) \end{bmatrix} = \begin{bmatrix} \frac{-1}{T_\sigma} & \omega_k & \frac{L_m}{\sigma L_S L_R T_R} & \frac{L_m}{\sigma L_S L_R} z_P \omega_m \\ -\omega_k & \frac{-1}{T_\sigma} & \frac{-L_m}{\sigma L_S L_R} z_P \omega_m & \frac{L_m}{\sigma L_S L_R T_R} \\ \frac{L_m}{T_R} & 0 & -\frac{1}{T_R} & (\omega_k - z_P \omega_m) \\ 0 & \frac{L_m}{T_R} & -(\omega_k - z_P \omega_m) & -\frac{1}{T_R} \end{bmatrix} \begin{bmatrix} \overrightarrow{i_{sa}}(t) \\ \overrightarrow{i_{sb}}(t) \\ \Psi_{Ra}(t) \\ \Psi_{Rb}(t) \end{bmatrix} + \begin{bmatrix} \frac{1}{\sigma L_S} & 0 \\ 0 & \frac{1}{\sigma L_S} \\ 0 & 0 \\ 0 & 0 \end{bmatrix} \cdot \begin{bmatrix} u_{Sa}(t) \\ u_{Sb}(t) \end{bmatrix} \tag{8}$$

The symbols appearing in (6) to (8) are defined as follows:

- $i_{Sa}(t), i_{Sb}(t)$ stator current components in the a and b axes at time t (A).
- $\Psi_{Ra}(t), \Psi_{Rb}(t)$ rotor flux linkage components in the a and b axes at time t (Wb).
- $\omega_k, \omega_m$ angular velocities: transformation and rotor (rad/s).
- $T_\sigma, T_R$ constants: related to leakage and rotor.
- $L_m, L_S, L_R$ inductances: magnetizing, stator, and rotor (H).
- $z_P$ number of pole pairs.
- $u_{Sa}(t), u_{Sb}(t)$ stator voltage components in the a and b axes at time t (V).
- $M_{mech}, M, M_L$ torques: mechanical, electromagnetic and load (Nm).
- J - inertia moment of the rotor (kg·m$^2$).
- σ - total leakage coefficient.

To validate the control strategy, the Lucas–Nuelle induction motor "SE2673-1K6" was selected. Its nameplate data are 220/380 V, 1.9/1.1 A, 60 Hz, 0.37 kW, 1650 rpm, and power factor of 0.76. The electrical and mechanical parameters used in the model are listed in Table 2. Employing manufacturer-specified values within the induction model block enhances the realism of the simulation and strengthens the correlation between numerical and experimental results.

Table 2. Lucas-Nuelle SE2673-1K6 electrical and mechanical parameters

| Symbol | Description | Units | Value |
|---|---|---|---|
| $L_r$ | Rotor inductance (related to the stator). | H | 1.3867 |
| $L_s$ | Stator inductance. | H | 1.3867 |
| $R_r$ | Rotor resistance. | Ω | 15.72 |
| $R_s$ | Stator resistance | Ω | 20.46 |
| $L_m$ | Magnetizing inductance | H | 1.3 |
| Inertia | Machine inertia | Kg m$^2$ | 0.0015 |
| Friction | The friction moment, which depends on the rotating speed | μ | 117e |
| $z_p$ | Machine pole number | | 4 |

## 2.2. PI control design

For PIC design, an operational speed range of 100–800 rpm is adopted, with the midpoint of 450 rpm chosen as the nominal operating condition. The controller gains are tuned by a PSO algorithm, which searches the parameter space to obtain a set of constants that minimize the defined cost function. The resulting PIC is implemented in a cascade configuration, as illustrated in Figure 3, where r(k) denotes the reference input, y(k) the measured speed output, e(k) the error, u(k) the control signal, and $u^{sat}(k)$ the saturated control signal applied to the plant. The saturation limits A and B and the sampling period Ts are explicitly shown to prevent windup [28]–[31], instability, and overcurrent conditions [32].

Figure 4 shows the closed-loop block diagram used to tune Kp and Ki on the MATLAB/Simulink platform. The PSO algorithm is coded in M-script and interacts with Simulink through iterative simulations. Its velocity and position updates in (10) and (11), respectively, and the fitness function minimizes the absolute speed error.

$$\vec{v}_i(t+1) = \omega\vec{v}_i(t) + c_1 r_1(\vec{p}_i(t) - \vec{x}_i(t)) + c_2 r_2(\vec{g}(t) - \vec{x}_i(t)) \quad (10)$$

$$\vec{x}_i(t+1) = \vec{x}_i(t) + \vec{v}_i(t+1) \quad (11)$$

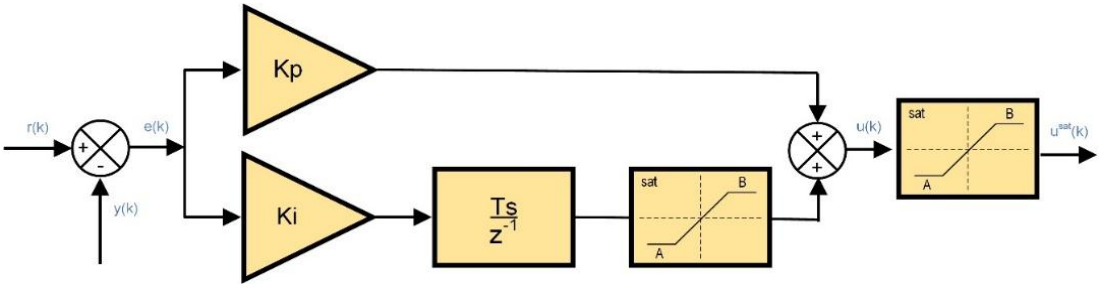


Figure 3. Cascade structure of a discrete PIC with anti-windup

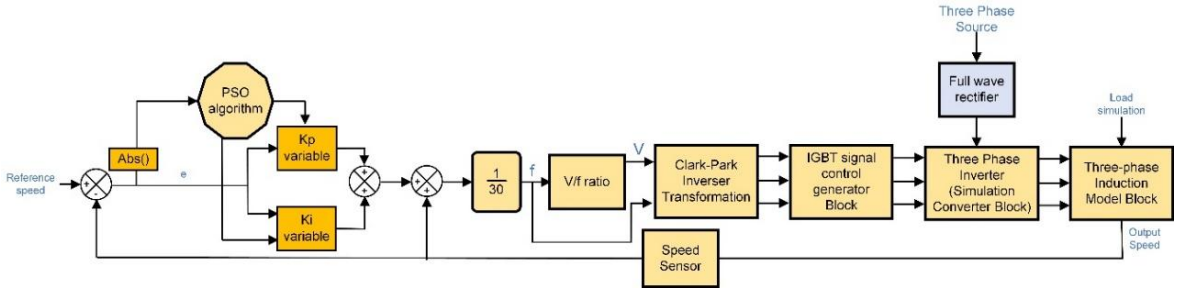


Figure 4. Closed-loop block diagram of V/f scalar of speed control

The swarm is configured with 15 particles, a maximum of 20 iterations, acceleration coefficients c1=c2=2, and an inertial factor that decreases linearly from ωmax=1 to ωmin=0.1. Random numbers r1 and r2 are uniformly drawn from [0,1] at every iteration to maintain search diversity. Under these settings, the algorithm returns Kp=0.6834 and Ki=0.7890 at the 450 rpm operating point; a subsequent fine adjustment yields final values of Kp=0.671 and Ki=0.750. After optimization, the PSO and Abs() blocks in

Figure 4 are removed, and the tuned Kp and Ki constants are hard-coded into the PIC, completing the controller-design procedure.

### 2.3. Fuzzy control design

For FC design, the PIC is first evaluated over the 100–800 rpm operating range, selecting several midpoints tuned with the PSO procedure. The resulting data provide expert-level knowledge that is encoded into fuzzy rules aimed at improving speed regulation performance with fuzzy logic. Design requirements are set to limit the inrush current peak to 1.52 A (≈ 80% of the rated current), confine the steady-state speed error to ±5 rpm, achieve a settling time below 1 s, and restrict both overshoot and undershoot to 15%.

Figure 5 provides an overview of the fuzzy-controller membership functions. The FC combines a Mamdani-type FLC with a conventional PIC whose gains Kp and Ki are adaptively selected by the FLC. The universe of discourse spans 100–800 rpm. The two inputs—reference speed and speed error—are mapped to triangular membership functions, while the two outputs—Kp and Ki—are likewise represented by triangular sets. As shown in Figure 5(a), speed is classified as low (LV), medium (MV), or high (HV); the velocity-error sets are small (SE), medium (ME), and large (LE). Figure 5(b) displays the output sets: small (SP), medium (MP), and large (LP) for Kp; and small (SI), medium (MI), and large (LI) for Ki. The rule base, summarized in Table 3, comprises nine "if–then" rules that use an AND conjunction, the minimum operator for implication, and the maximum operator for aggregation. Following aggregation, the centroid method is applied for defuzzification, yielding crisp values of Kp and Ki that satisfy the aforementioned performance criteria.

Both the FLC and the discrete PI control law are implemented in a MATLAB function block within the MATLAB/Simulink environment. The PI equation is coded in difference form, and an anti-windup limiter—implemented by saturating the control variable between ±A and ±B—prevents windup, instability, and overcurrent. Figure 1 presents the complete closed-loop diagram of the system governed by the FC.

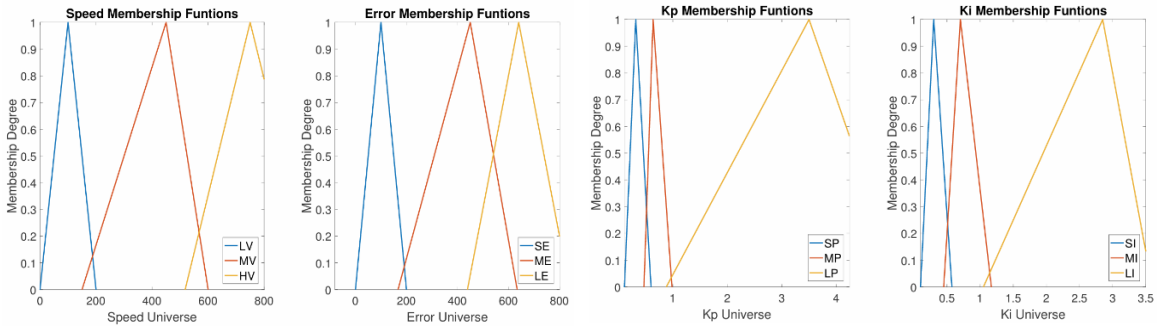


(a) (b)

Figure 5. Fuzzy controller membership functions: (a) input and (b) output

Table 3. Fuzzy controller rules

| V\e | SE | ME | LE |
|---|---|---|---|
| LV | LP/LI | MP/MI | SP/SI |
| MV | MP/MI | MP/MI | SP/SI |
| HV | SP/SI | MP/MI | SP/SI |

## 3. RESULTS AND DISCUSSION

Closed-loop responses of the V/f scalar control scheme were evaluated at reference speeds of 100, 250, 400, 575, and 750 rpm under load torques of 0.19, 0.24, and 0.41 Nm. Both the PIC and the FC were tested to enable a direct comparison. Figures 6 to 8 show dynamic behavior for three representative operating points. Figure 6(a) displays the speed response; Figure 6(b) the inrush current; and Figure 6(c) the permanent current—all at 100 rpm with a 0.19 Nm load. Similarly, Figure 7 presents the same responses at a 250 rpm reference with a 0.24 Nm load, while Figure 8 shows the same responses at a 100 rpm reference with a 0.21 Nm load.

Tables 4 and 5 list the principal response indices—undershoot, undershoot time, settling time, inrush-current RMS, and permanent-current RMS—across the five reference speeds noted above under the specified load levels. Table 6 condenses these data into performance differentials between the two controllers, while Table 7 summarizes the transient parameters and their variation in the low-speed robustness test conducted at 100 rpm and 0.21 Nm, based on the dynamic behavior shown in Figure 8. The robustness scenarios depicted

in Figure 8 and Table 7 deliberately exceed the original design constraints and illustrate each controller's behavior under demanding conditions.

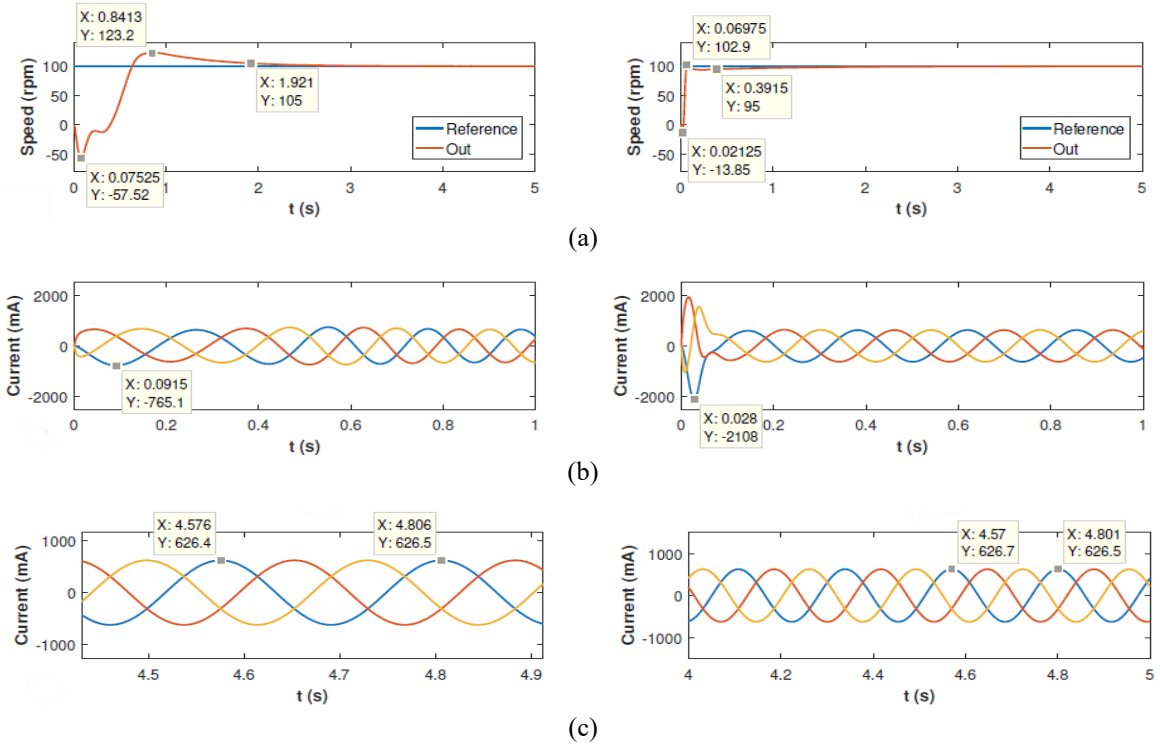


Figure 6. The first and second columns present the PIC and FC responses respectively at 100 rpm and 0.19 Nm: (a) speed, (b) start-up current, and (c) steady-state current

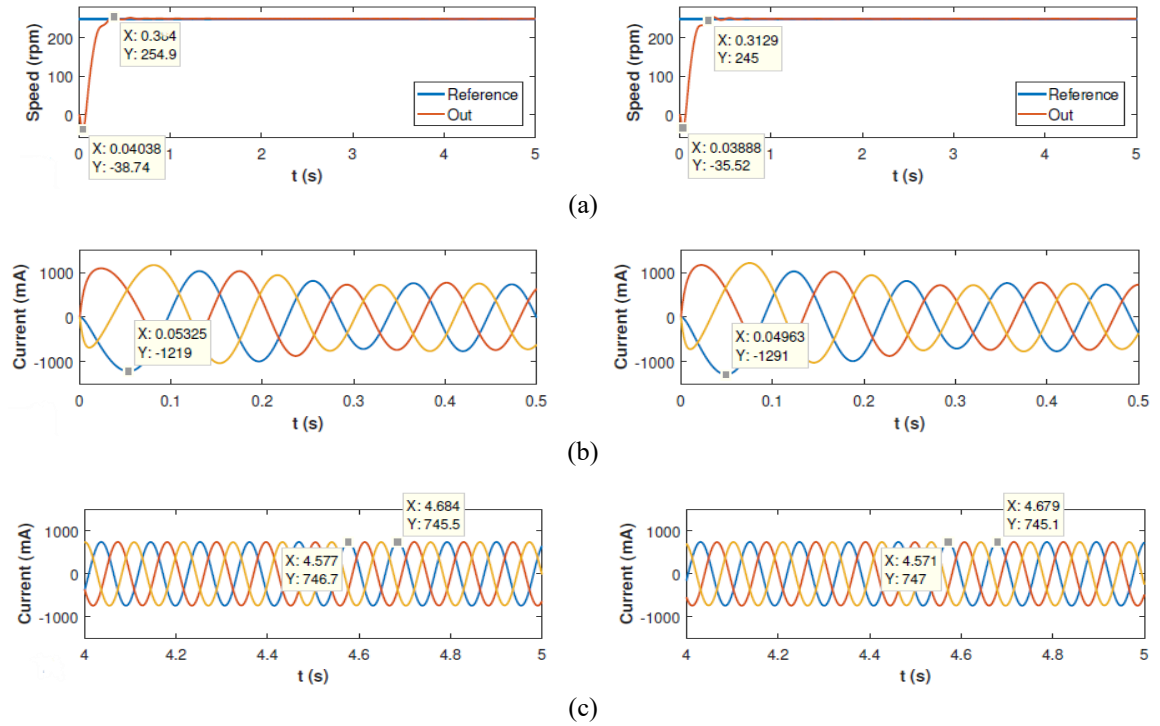


Figure 7. The first and second columns present the PIC and FC responses respectively at 250 rpm and 0.24 Nm: (a) speed, (b) start-up current, and (c) steady-state current

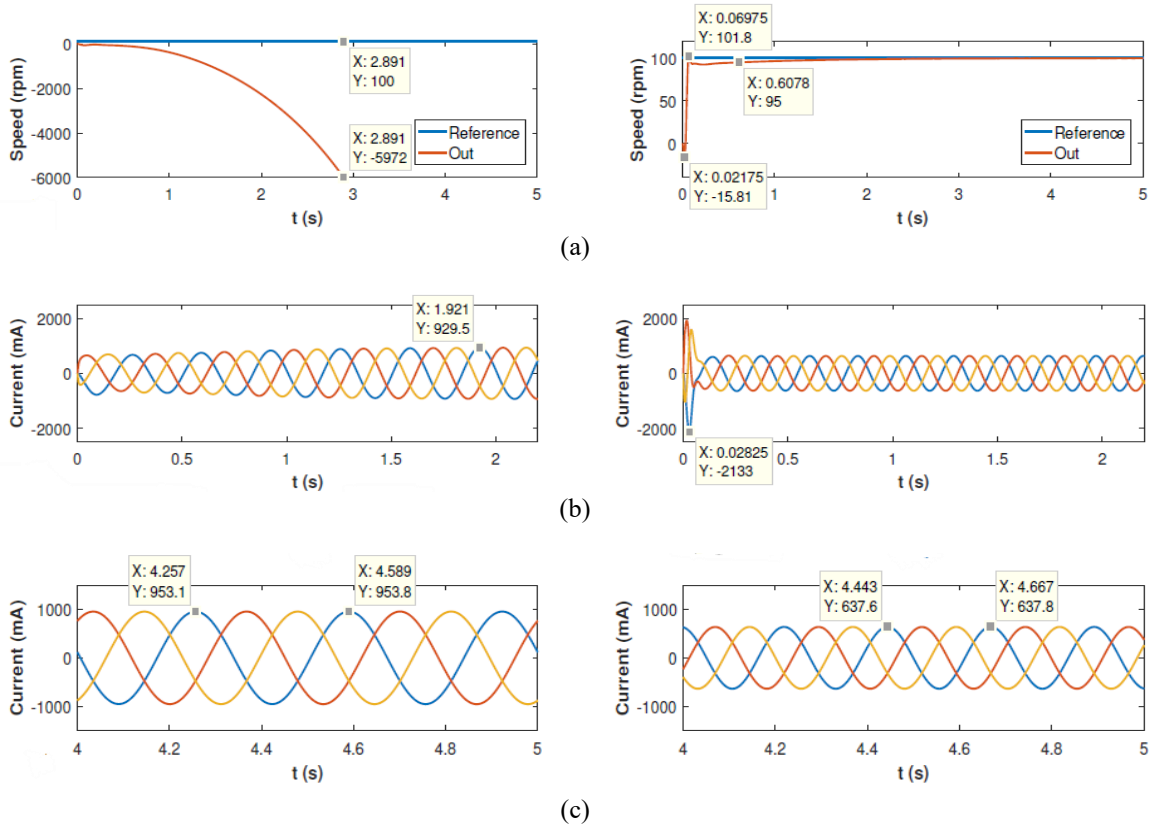


Figure 8. The speed robustness test at low speed (100 rpm and 0.21 Nm): (a) speed, (b) start-up current, and (c) steady-state current

Table 4. Speed and current response parameters at 100, 250, and 400 rpm

| Parameter | PIC | FC | PIC | FC | PIC | FC |
|---|---|---|---|---|---|---|
| Reference velocity [rpm] | 100 | | 250 | | 400 | |
| Load [Nm] | 0.19 | | 0.24 | | 0.41 | |
| Undershoot [%] | 57.52 | 13.85 | 15.50 | 14.20 | 11.92 | 11.12 |
| Undershoot time [s] | 0.08 | 0.02 | 0.04 | 0.04 | 0.03 | 0.03 |
| Setting time [s] | 1.92 | 0.39 | 0.38 | 0.31 | 0.85 | 0.72 |
| Inrush current RMS [mA] | 541.01 | 1490.58 | 861.96 | 912.87 | 1286.23 | 1335.02 |
| Permanent current RMS [mA] | 443.00 | 443.14 | 528.00 | 528.21 | 623.67 | 623.46 |

Table 5. Speed and current response parameters at 575 and 750 rpm

| Parameter | PIC | FC | PIC | FC |
|---|---|---|---|---|
| Reference velocity [rpm] | 575 | | 750 | |
| Load [Nm] | 0.41 | | 0.41 | |
| Undershoot [%] | 6.36 | 6.93 | 4.80 | 6.59 |
| Undershoot time [s] | 0.02 | 0.02 | 0.02 | 0.03 |
| Setting time [s] | 0.43 | 0.29 | 2.33 | 0.43 |
| Inrush current RMS [mA] | 1668.77 | 1459.47 | 1999 | 1377.444 |
| Permanent current RMS [mA] | 634.77 | 626.921 | 656.9 | 659.5892 |

Table 6. Parameters comparison between controllers

| Parameter | Controllers variations | | | | |
|---|---|---|---|---|---|
| Reference velocity [rpm] | 100 | 250 | 400 | 575 | 750 |
| Load [Nm] | 0.19 | 0.24 | 0.41 | 0.41 | 0.41 |
| Undershoot [%] | 43.67 | 1.3 | 0.8 | -0.57 | -1.79 |
| Undershoot time [s] | 0.05 | 0.00 | 0.00 | 0.00 | -0.01 |
| Setting time [s] | 1.53 | 0.07 | 0.13 | 0.14 | 1.90 |
| Inrush current RMS [mA] | -949.57 | -50.91 | -48.79 | 209.30 | 621.55 |
| Permanent current RMS [mA] | -0.14 | -0.21 | 0.21 | 7.85 | -2.69 |

Table 7. Robustness test parameters at low speeds

| Parameter/Controller | PIC | FC | Variation |
|---|---|---|---|
| Reference velocity [rpm] | | 100 | |
| Load [Nm] | | 0.21 | |
| Undershoot [%] | undetermined | 15.81 | Not comparable |
| Undershoot time [s] | undetermined | 0.02 | Not comparable |
| Setting time [s] | Not stable | 0.61 | Not comparable |
| Inrush current RMS [mA] | 657.26 | 1508.26 | -851.00 |
| Permanent current RMS [mA] | 674.44 | 450.99 | 223.45 |

A comparative analysis between the FC and the PIC under identical design constraints confirms the FC's superior transient performance and robustness. Across the full speed span—from 100 to 800 rpm—the FC shortens settling time by up to 1.53 s at 100 rpm and by 1.90 s at 750 rpm, while keeping the steady-state speed within ±5 rpm (Figures 6 and 7; Tables 4 to 6). These findings align with earlier studies showing that FC enhances the dynamic response of induction motor drives at medium, rated, and above-rated speeds [20]–[22], while the present work extends this evidence by validating a conventional PI-based scalar V/f control scheme at very low speeds.

Start-up current offers another clear distinction. Throughout the entire test range, the FC keeps the inrush current below the 1.52 A design ceiling as can be seen in Figures 6(b) and 7(b)—even though torque boost raises current demand at low speeds—whereas the PIC approaches or surpasses that threshold at several points. At 100 rpm, the torque-boost action eliminates the overshoot (23.2%) and reduces the extreme undershoot (57.52%) recorded with the PIC (Figure 6 and Table 4). This prevents the two-second stabilization delay that renders the PIC response unacceptable. Adaptive fuzzy schemes have demonstrated reductions in overshoot and stabilization time [21]; however, the improvements in low-speed control observed in this work exceed those of previous studies.

Although the FC occasionally registers undershoot values marginally higher than those of the PIC (≤ 1.79%), these excursions remain well within the design limit, whereas the PIC violates it at 100 rpm (57.52%) and 250 rpm (15.50%) represented in Figures 6(a) and 7(a). Such undershoot magnitudes undermine optimal control performance. Moreover, across the evaluated range, the PIC exhibits the highest peak undershoot time—four times that of the FC. Hence, both techniques maintain adequate steady-state current behavior without producing side effects during continuous operation, see Figure 6(c) and 7(c).

The low-speed robustness test at 100 rpm and 0.21 Nm (Figure 8 and Table 7) exposes a critical difference in the same parameters analyzed above for the two control strategies. Although the PIC shows apparently adequate current waveforms—both during start-up and in steady state as shown in Figure 8(b) and Figure 8(c) it drives the speed response into an unrecoverable collapse, indicating an insufficient stability margin under even modest load disturbances, which is observed in Figure 8(a). By contrast, the FC maintains a peak-undershoot time comparable to the other speed cases, keeps the inrush current below the 1.52 A design limit, and achieves a stabilization pattern that mirrors the speed robustness reported for fuzzy schemes in previous studies [22], thereby demonstrating an acceptable level of robustness at low speed.

As a result, within a robustness margin of 0.21 Nm, the PIC must be ruled out, whereas the FC delivers a tolerable response; its only deviation from the specifications is an undershoot that exceeds the target by just 0.81%. This minor deviation could be eliminated by fine-tuning the fuzzy rule set or adjusting the membership-function boundaries. Overall, this comparison confirms that the FC retains acceptable robustness across the entire speed range, while the PIC's performance deteriorates sharply as operating conditions deviate from those analyzed.

To extend the discussion beyond the transient responses and robustness test, Figure 9 examines a ±50 rpm speed-tracking test at 100 rpm under a 0.19 Nm load, where Figure 9(a) shows the speed dynamic response. Relative to the PIC, the FC reduces start-up overshoot and undershoot by 83.66% and 76%, respectively, and shortens the settling time by 0.831 s for the upward step and 0.719 s for the downward step. The FC also confines the overshoot and undershoot duration to only 26 ms—an order of magnitude faster than the PIC—thereby sustaining tight speed regulation even during rapid set-point changes. On the other hand, Figure 9(b) examines the transient behavior of the current, where the FC's starting current reaches at most 1.49 A. Despite the repetitive speed changes, the FC current maintains the same performance improvements. This result corroborates the scope of the FC's robustness and transient responses observed at low speed and mirrors the fast-adaptation behavior reported for fuzzy schemes at higher speeds in previous studies, while also demonstrating the enhanced starting performance achieved in this research—further highlighting the FC's superior agility, stability, and overall performance compared with the PIC.

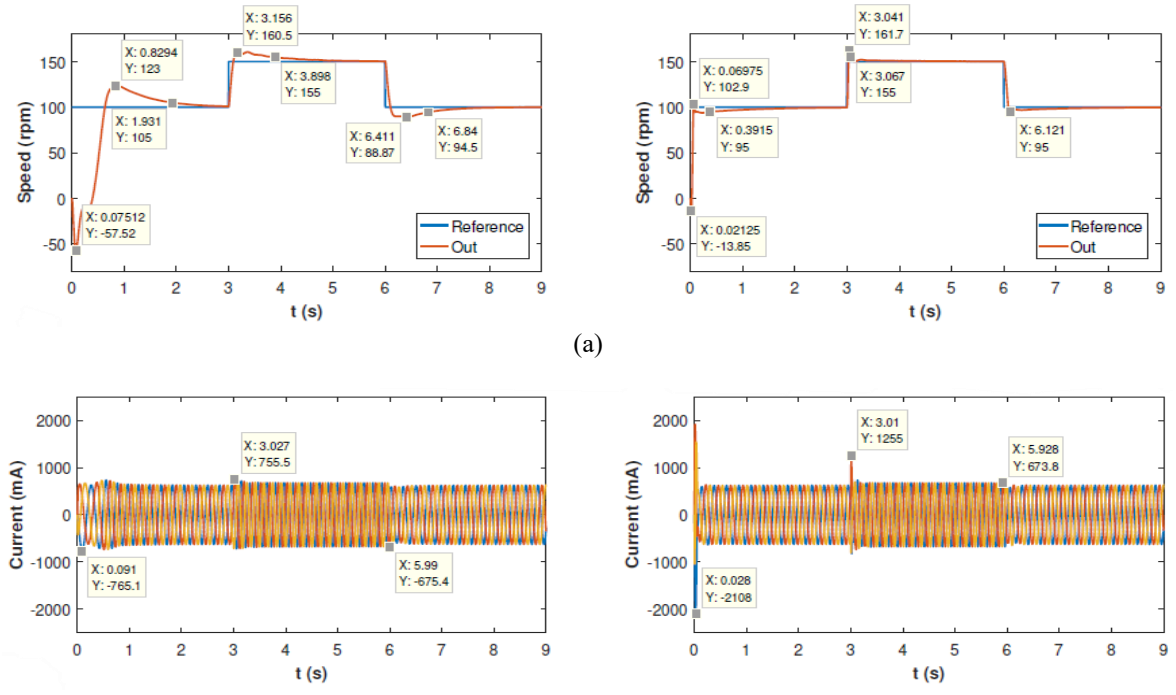


Figure 9. The first and second columns present the PIC and FC responses, respectively, in the low-speed variation test at 100 rpm and 0.19 Nm: (a) speed and (b) current

## 4. CONCLUSION

This work presented a comparative analysis between PIC and FC in V/f scalar speed control of a TIM at low speeds, supported by simulations conducted in MATLAB/Simulink using Lucas-Nülle's toolbox for precise modeling. The results confirm that the integration of fuzzy logic significantly enhances speed regulation not only at low speeds but also across medium ranges, yielding superior dynamic performance. The FC achieved zero overshoot within a ±2.9 rpm stability margin, reduced stabilization time by up to 0.29 s under different load conditions, and limited the starting current to below 76.8% of the motor's rated value, ensuring efficient control across the low-frequency region. Compared with the PIC, the FC consistently delivered better speed tracking and inrush-current mitigation, enabling operation at just 6.06% of rated speed while maintaining favorable transient characteristics under load. Future efforts will focus on implementing these control strategies in a physical setup to validate the simulation results under real operating scenarios, as well as refining the fuzzy rule base and membership functions to further enhance robustness and overall efficiency.

## ACKNOWLEDGMENTS

This research was supported by the Institutional Laboratory for Research, Entrepreneurship, and Innovation in Automatic Control Systems, Automation, and Robotics (LIECAR) and the Laboratory of Renewable Energies, Optical Communications Engineering, and Environmental Technology (TESLA) at the Universidad Nacional de San Antonio Abad del Cusco (UNSAAC). We also sincerely thank Roy D. Peña Alegre for his valuable contribution to the development of this research article.

## FUNDING INFORMATION

Authors state no funding involved.

## AUTHOR CONTRIBUTIONS STATEMENT

This journal uses the Contributor Roles Taxonomy (CRediT) to recognize individual author contributions, reduce authorship disputes, and facilitate collaboration.

| Name of Author | C | M | So | Va | Fo | I | R | D | O | E | Vi | Su | P | Fu |
|---|---|---|---|---|---|---|---|---|---|---|---|---|---|---|
| Alfonso Alejandro Sevilla-Hidalgo | ✓ | ✓ | ✓ | ✓ | ✓ | ✓ | | ✓ | ✓ | ✓ | ✓ | | | |
| Rossy Uscamaita-Quispetupa | ✓ | ✓ | ✓ | ✓ | ✓ | ✓ | | ✓ | | ✓ | ✓ | | | |
| Julio Cesar Herrera-Levano | ✓ | | | | | ✓ | ✓ | | | ✓ | ✓ | | | |
| Limberg Walter Utrilla Mego | ✓ | | | | ✓ | | ✓ | | | ✓ | ✓ | ✓ | | |
| Roger Jesus Coaquira-Castillo | ✓ | ✓ | | ✓ | ✓ | ✓ | ✓ | | ✓ | ✓ | ✓ | ✓ | ✓ | |

C : **C**onceptualization
M : **M**ethodology
So : **So**ftware
Va : **Va**lidation
Fo : **Fo**rmal analysis
I : **I**nvestigation
R : **R**esources
D : **D**ata Curation
O : Writing - **O**riginal Draft
E : Writing - Review & **E**diting
Vi : **Vi**sualization
Su : **Su**pervision
P : **P**roject administration
Fu : **Fu**nding acquisition

## CONFLICT OF INTEREST STATEMENT

Authors state no conflict of interest.

## DATA AVAILABILITY

The authors confirm that the data supporting the findings of this study are available within the article.

## REFERENCES


[1] A. F. Abouzeid *et al.*, "Control strategies for induction motors in railway traction applications," *Energies*, vol. 13, no. 3, 2020, doi: 10.3390/en13030700.

[2] A. Choudhary, D. Goyal, S. L. Shimi, and A. Akula, "Condition monitoring and fault diagnosis of induction motors: A review," *Archives of Computational Methods in Engineering*, vol. 26, no. 4, pp. 1221–1238, 2019, doi: 10.1007/s11831-018-9286-z.

[3] D. F. de Souza, F. A. M. Salotti, I. L. Sauer, H. Tatizawa, A. T. de Almeida, and A. G. Kanashiro, "A performance evaluation of three-phase induction electric motors between 1945 and 2020," *Energies*, vol. 15, no. 6, 2022, doi: 10.3390/en15062002.

[4] R. Bharti, M. Kumar, and B. M. Prasad, "V/F control of three phase induction motor," in *2019 International Conference on Vision Towards Emerging Trends in Communication and Networking (ViTECoN)*, 2019, pp. 1–4, doi: 10.1109/ViTECoN.2019.8899420.

[5] R. M. -Capora, G. M. -Gomez, A. P. -López, K. E. H. -Castañeda, and F. A. V. -Tonix, "Design of a three-phase inverter and implementation of scalar control to drive an induction motor with applications in electric vehicles (In Spanish: *Diseño de un inversor trifásico e implementación del control escalar para accionar una máquina de inducción con aplicaciones en vehículos eléctricos*)," *Memorias del Congreso Internacional de Investigación Academia Journals Celaya 2016*, vol. 8, no. 5, pp. 3999–4004, 2016.

[6] Z. Zhang and A. M. Bazzi, "Robust sensorless scalar control of induction motor drives with torque capability enhancement at low speeds," in *2019 IEEE International Electric Machines & Drives Conference (IEMDC)*, 2019, pp. 1706–1710, doi: 10.1109/IEMDC.2019.8785159.

[7] M. Habyarimana, D. G. Dorrell, and R. Musumpuka, "Reduction of starting current in large induction motors," *Energies*, vol. 15, no. 10, 2022, doi: 10.3390/en15103848.

[8] G. A. Olarinoye, C. Akinropo, G. J. Atuman, and Z. M. Abdullahi, "Speed control of a three phase induction motor using a PI controller," in *2019 2nd International Conference of the IEEE Nigeria Computer Chapter (NigeriaComputConf)*, 2019, pp. 1–7, doi: 10.1109/NigeriaComputConf45974.2019.8949624.

[9] M. Hashem, M. Abdel-Salam, M. Nayel, and M. T. El-Mohandes, "Mitigation of voltage sag in a distribution system during start-up of water-pumping motors using superconducting magnetic energy storage: A case study," *Journal of Energy Storage*, vol. 55, 2022, doi: 10.1016/j.est.2022.105441.

[10] H. A.-J. Al-Asady and H. F. Fakhruldeen, "Volts/Hz control of three-phase induction machine: MATLAB Simulink," *Journal of Physics: Conference Series*, vol. 1818, no. 1, 2021, doi: 10.1088/1742-6596/1818/1/012089.

[11] H. M. D. Habbi, H. J. Ajeel, and I. I. Ali, "Speed control of induction motor using PI and V/F scalar vector controllers," *International Journal of Computer Applications*, vol. 151, no. 7, pp. 36–43, 2016, doi: 10.5120/ijca2016911831.

[12] R. Errouissi, A. Al-Durra, and S. M. Muyeen, "Experimental validation of a novel PI speed controller for AC motor drives with improved transient performances," *IEEE Transactions on Control Systems Technology*, vol. 26, no. 4, pp. 1414–1421, 2018, doi: 10.1109/TCST.2017.2707404.

[13] I. D. D. -Rodríguez, S. Han, and S. P. Bhattacharyya, "Introduction to control," in *Analytical Design of PID Controllers*, Cham, Switzerland: Springer, 2019, pp. 1–34, doi: 10.1007/978-3-030-18228-1_1.

[14] A. Srivastav, M. Rizwan, and V. K. Yadav, "Comparative analysis of conventional and intelligent methods for speed control of induction motor," in *Control Applications in Modern Power Systems*, Singapore: Springer, 2023, pp. 63–75, doi: 10.1007/978-981-19-7788-6_5.

[15] O. Rabiaa, B. H. Mouna, D. Mehdi, and S. Lassaad, "Scalar speed control of dual three phase induction motor using PI and IP controllers," in *2017 International Conference on Green Energy Conversion Systems (GECS)*, 2017, pp. 1–6, doi: 10.1109/GECS.2017.8066225.

[16] M. A. Hannan, J. A. Ali, A. Mohamed, and A. Hussain, "Optimization techniques to enhance the performance of induction motor drives: A review," *Renewable and Sustainable Energy Reviews*, vol. 81, pp. 1611–1626, Jan. 2018, doi: 10.1016/j.rser.2017.05.240.
[17] A. Gupta, L. Mathew, and S. Chatterji, "V/f-based speed controllers for an induction motor using AI techniques: A comparative analysis," in *Proceedings of the Second International Conference on Soft Computing for Problem Solving (SocProS 2012)*, 2014, pp. 1161–1171, doi: 10.1007/978-81-322-1602-5_122.
[18] E. V. Morozova, A. N. Samoilenko, R. V. Baranouski, and A. S. Morozova, "An induction motor control system based on artificial intelligence," in *2020 XXIII International Conference on Soft Computing and Measurements (SCM)*, 2020, pp. 76–79, doi: 10.1109/SCM50615.2020.9198812.
[19] H. Salahuddin, K. Imdad, M. U. Chaudhry, D. Nazarenko, V. Bolshev, and M. Yasir, "Induction machine-based EV vector control model using Mamdani fuzzy logic controller," *Applied Sciences*, vol. 12, no. 9, pp. 1-19, May. 2022, doi: 10.3390/app12094647.
[20] K. Santhiya, M. Devimuppudathi, D. S. Kumar, and A. J. Renold, "Real time speed control of three phase induction motor by using lab view with fuzzy logic," *Journal on Science Engineering and Technology*, vol. 5, no. 2, pp. 21–27, 2018.
[21] N. H. Mugheri and M. U. Keerio, "An optimal fuzzy logic-based PI controller for the speed control of an induction motor using the V/F method," *Engineering, Technology & Applied Science Research*, vol. 11, no. 4, pp. 7399–7404, 2021, doi: 10.48084/etasr.4255.
[22] S. C. Rajpoot, N. K. Soni, S. Shrivastava, and P. S. Rajpoot, "Speed control of three phase motor using fuzzy logic controller," *International Research Journal of Engineering and Technology (IRJET)*, vol. 5, no. 10, pp. 478–486, 2018.
[23] S. Kesler, "Performance analysis of different PWM techniques on V/f-based speed control with adjustable boost voltage application for induction motors," *Pamukkale University Journal of Engineering Sciences*, vol. 24, no. 5, pp. 797–808, 2018, doi: 10.5505/pajes.2018.13845.
[24] N. S. Ramadhan, I. Ferdiansyah, and E. Purwanto, "Voltage booster for optimizing scalar control methods on single passenger electric vehicles," in *2022 Fifth International Conference on Vocational Education and Electrical Engineering (ICVEE)*, 2022, pp. 174–177, doi: 10.1109/ICVEE57061.2022.9930374.
[25] R. Krishnan, "Polyphase induction machines," in *Electric Motor Drives: Modeling, Analysis, and Control,* Upper Saddle River, United States: Prentice Hall, 2001.
[26] K. A. M. Annuar, M. R. M. Sapiee, R. M. Nor, M. S. M. Azali, M. B. N. Shah, and S. M. Rozali, "Squirrel cage induction motor scalar control constant V/F analysis," *TELKOMNIKA (Telecommunication Computing Electronics and Control)*, vol. 17, no. 1, pp. 417–424, 2019, doi: 10.12928/TELKOMNIKA.v17i1.8818.
[27] L. -Nuelle, "Electromechanical energy conversion – transformers – machines – power electronics," *Lucas-Nuelle US.* 2023. [Online]. Available: https://www.lucas-nuelle.us/2756/apg/2/Products/Electromechanical-Energy-Conversion-%7C-Transformers-%7C-Machines-%7C-Power-Electronics.htm
[28] MathWorks, "PI controller with integral anti-windup (discrete or continuous)," *The Mathworks Inc.* 2025. [Online]. Available: https://se.mathworks.com/help/sps/ref/discretepicontroller.html
[29] J. R. B. A. Monteiro, W. C. A. Pereira, M. P. Santana, T. E. P. Almeida, G. T. Paula, and I. Santini, "Anti-windup method for fuzzy PD+I, PI and PID controllers applied in brushless DC motor speed control," in *2013 Brazilian Power Electronics Conference*, 2013, pp. 865–871, doi: 10.1109/COBEP.2013.6785216.
[30] W. Gharieb and G. Nagib, "Fuzzy intervention in PID controller design," in *2001 IEEE International Symposium on Industrial Electronics Proceedings*, 2001, pp. 1639–1643, doi: 10.1109/isie.2001.931953.
[31] A. Hansson, P. Gruber, and J. Tödtli, "Fuzzy anti-reset windup for PID controllers," *IFAC Proceedings Volumes*, vol. 26, no. 2, pp. 917–920, 1993, doi: 10.1016/S1474-6670(17)48407-2.
[32] A. M. Trzynadlowski, "Scalar control methods," in *Control of Induction Motors*, Elsevier, 2001, pp. 93–105, doi: 10.1016/B978-012701510-1/50005-2.

## BIOGRAPHIES OF AUTHORS

**Alfonso Alejandro Sevilla-Hidalgo** received the Electronic Engineering degree from the National University of San Antonio Abad of the Cusco, Peru. He is currently working in the field of biomedical engineering, providing services to hospitals and healthcare institutions. His work covers healthcare facilities of primary, secondary, and tertiary levels, performing preventive, corrective, and predictive maintenance of biomedical equipment and electrical infrastructure. Since 2021, he has been involved in project development, consulting, and technical documentation in hospital engineering. Moreover, since 2022, he has been working in the areas of control, automation, and telecommunications. He can be contacted at email: 160345@unsaac.edu.pe.

**Rossy Uscamaita-Quispetupa** received the master's degree in Control and Automation Engineering from the Pontificia Universidad Catolica del Peru (PUCP) and the bachelor's degree in Electronic Engineering from the Universidad Nacional de San Antonio Abad del Cusco (UNSAAC). She has participated in various applied research projects funded by ISA-REP, CONCYTEC at PUCP, and UNSAAC. She has also received training in Project Management, Logistics, Industrial Networks, CCNA, Generating Sets, and PLC Programming. She is currently a Professor at the Universidad Nacional de San Antonio Abad del Cusco (UNSAAC). Additionally, she is a member of IEEE, part of the AESS chapter. She can be contacted at email: rossy.uscamaita@unsaac.edu.pe.

**Julio Cesar Herrera-Levano** is an Electronic Engineer from the Universidad Nacional del Callao, and Master in Science, Electronic Engineering with specialization in Automation and Instrumentation from the Universidad Nacional San Agustín. He is a RENACYT Researcher Level V and has been a professor at the Professional School of Electronic Engineering at the Universidad Nacional de San Antonio de Abad del Cusco (UNSAAC) since 2014. With 25 years of experience in telecommunication. Participating in research projects funded by the Special Fund for University Development (FEDU), he has contributed to the spectral analysis of mobile telephony and the evaluation of SDR devices. He can be contacted at email: julio.herrera@unsaac.edu.pe.

**Limberg Walter Utrilla Mego** holds a Dr. in Mechatronics Engineering, a Master of Science in Electronic Engineering with a major in Automation and Instrumentation from the Universidad Nacional San Agustín, and a Professional Degree in Electronic Engineering from the Antenor Orrego Private University. He currently works as a Specialty Professor at the Professional School of Electronic Engineering at the Universidad Nacional de San Antonio Abad del Cusco. He is currently the director of the Renewable Energy, Optical Communications Engineering and Environmental Technology Laboratory (TESLA). He can be contacted at email: walter.mego@unsaac.edu.pe.

**Roger Jesus Coaquira-Castillo** received a Master of Science degree in Automation and Instrumentation from the Universidad Nacional de Ingenieria (UNI) in 2020 and a degree of doctor in Environment and Sustainable Development from the Universidad Andina del Cusco (UAC) in 2023. He is a RENACYT Researcher Level IV, he is currently a full professor at the Universidad Nacional de San Antonio Abad del Cusco (UNSAAC), Cusco, Peru. He is currently the Vice Director of the Institutional Laboratory for Research, Entrepreneurship, and Innovation in Automatic Control Systems, Automation and Robotics (LIECAR). His main research interests include artificial intelligence, automatic control, robotics, and industrial automation. He can be contacted at email: roger.coaquira@unsaac.edu.pe.